TECHNICAL ADVANCE

Global Change Biology WILEY

Deep learning to extract the meteorological by-catch of wildlife cameras

Jamie Alison[1] | Stephanie Payne[2] | Jake M. Alexander[3] | Anne D. Bjorkman[4,5] | Vincent Ralph Clark[6] | Onalenna Gwate[6] | Maria Huntsaar[7,8] | Evelin Iseli[3] | Jonathan Lenoir[9] | Hjalte Mads Rosenstand Mann[1,10] | Sandy-Lynn Steenhuisen[2] | Toke Thomas Høye[1,10]

[1]Department of Ecoscience, Aarhus University, Aarhus, Denmark

[2]Afromontane Research Unit and Department of Plant Sciences, University of the Free State, Bloemfontein, South Africa

[3]Institute of Integrative Biology, ETH Zurich, Zurich, Switzerland

[4]Department of Biological and Environmental Sciences, University of Gothenburg, Gothenburg, Sweden

[5]Gothenburg Global Biodiversity Centre, Gothenburg, Sweden

[6]Afromontane Research Unit and Department of Geography, University of the Free State, Bloemfontein, South Africa

[7]Arctic Biology Department, The University Centre in Svalbard (UNIS), Longyearbyen, Norway

[8]Department of Arctic and Marine Biology, The Arctic University of Norway (UiT), Tromsø, Norway

[9]UMR CNRS 7058 "Ecologie et Dynamique des Systèmes Anthropisés" (EDYSAN), Université de Picardie Jules Verne, Amiens, France

[10]Arctic Research Centre, Aarhus University, Aarhus, Denmark

Correspondence
Jamie Alison, Department of Ecoscience, Aarhus University, Aarhus, Denmark.
Email: jalison@ecos.au.dk

Funding information
Department of Science and Innovation, South Africa, Grant/Award Number: DSI/CON 0000/2021; Innovationsfonden, Grant/Award Number: 0156-00022B; Schweizerischer Nationalfonds zur

Abstract

Microclimate—proximal climatic variation at scales of metres and minutes—can exacerbate or mitigate the impacts of climate change on biodiversity. However, most microclimate studies are temperature centric, and do not consider meteorological factors such as sunshine, hail and snow. Meanwhile, remote cameras have become a primary tool to monitor wild plants and animals, even at micro-scales, and deep learning tools rapidly convert images into ecological data. However, deep learning applications for wildlife imagery have focused exclusively on living subjects. Here, we identify an overlooked opportunity to extract latent, ecologically relevant meteorological information. We produce an annotated image dataset of micrometeorological conditions across 49 wildlife cameras in South Africa's Maloti-Drakensberg and the Swiss Alps. We train ensemble deep learning models to classify conditions as overcast, sunshine, hail or snow. We achieve 91.7% accuracy on test cameras not seen during training. Furthermore, we show how effective accuracy is raised to 96% by disregarding 14.1% of classifications where ensemble member models did not reach a consensus. For two-class weather classification (overcast vs. sunshine) in a novel location in Svalbard, Norway, we achieve 79.3% accuracy (93.9% consensus accuracy), outperforming a benchmark model from the computer vision literature (75.5% accuracy). Our model rapidly classifies sunshine, snow and hail in almost 2 million unlabelled images. Resulting micrometeorological data illustrated common seasonal patterns of summer hailstorms and autumn snowfalls across mountains in the northern and southern hemispheres. However, daily patterns of sunshine and shade diverged between sites, impacting daily temperature cycles. Crucially, we leverage micrometeorological data to demonstrate that (1) experimental warming using open-top chambers shortens early snow events in autumn, and (2) image-derived sunshine marginally outperforms sensor-derived temperature when predicting bumblebee foraging. These methods generate novel micrometeorological variables in synchrony with biological recordings, enabling new insights from an increasingly global network of wildlife cameras.

1 | INTRODUCTION

Climate change is redistributing species in space and time, with profound impacts on ecosystem function and human wellbeing (Pecl et al., 2017). While biodiversity impacts of climate change are usually reported at coarse spatial resolutions across large spatial extents (Lenoir et al., 2020), species often respond to climate at much finer scales (Lembrechts et al., 2019; Maclean & Early, 2023; Potter et al., 2013). Furthermore, studies of the biodiversity impacts of climate change are traditionally temperature centric (Antão et al., 2020). As the study of microclimate has expanded, this temperature centricity has remained (Maclean et al., 2021), due in part to the availability of inexpensive and easy-to-use temperature loggers (Lembrechts et al., 2020). Still, non-temperature aspects of climate and meteorology have profound, fine-scale impacts on species and communities. Solar radiation (i.e. sunshine) not only underpins ambient temperature, but also directly impacts plant growth and animal behaviour (Möhl et al., 2020; Roales et al., 2013; Valladares et al., 2016). Furthermore, snow cover severely constrains the onset of plants' growing and flowering seasons (Möhl et al., 2022), impacting plant–pollinator interactions (Gillespie et al., 2016; Gillespie & Cooper, 2022). Hail receives very little attention in ecological research, yet presents a direct physical threat that can devastate poorly adapted plant species (Fernandes et al., 2011). As the frequency of extreme weather events increases (IPCC, 2023), it is vital that sensor networks capture not only temperature, but also a range of other fine-scale meteorological variables.

Meanwhile, novel technology is revolutionizing the monitoring of ecological communities, generating data with unprecedented temporal continuity and resolution (August et al., 2015; Besson et al., 2022). Wildlife cameras—in situ autonomous cameras that record wildlife—are particularly promising. Camera traps are an established method to monitor large animals (Burton et al., 2015), but wildlife cameras are now regularly deployed to study small mammals and birds (Ortmann & Johnson, 2021), insects and other arthropods (Høye et al., 2021) and plants (Katal et al., 2022). For vegetation, the 'PhenoCam' approach has gained traction, capturing community-level characteristics such as plant productivity (Brown et al., 2016). However, the volume of images from wildlife cameras has proven difficult to manage, so algorithms are being developed to automatically extract ecological data (Høye et al., 2021; Tuia et al., 2022). Deep learning models are a prevalent family of algorithms used to detect, classify and track animals in images (Norouzzadeh et al., 2018). For plants, algorithms can be trained to flag phenological events such as the onset of budburst or flowering (Katal et al., 2022), or to detect and track individual flowers (Mann et al., 2022).

The consistency of image-based monitoring allows for incidental recording of non-target biota, known as 'by-catch'. For example, a camera trap network intended to study the Eurasian lynx in the Swiss Jura mountains has proven useful to explore habitat use by wild boar and roe deer (Wevers et al., 2021). However, it is increasingly recognized that wildlife cameras also capture non-target abiotic information, including meteorological conditions not easily captured with alternative sensors (Hofmeester et al., 2020). Furthermore, capturing both biotic and abiotic data with a single sensor ensures that they are measured simultaneously, at equivalent spatial and temporal scales. Several studies have manually extracted the presence, cover or depth of snow in ecological imagery (Lumbrazo et al., 2022). Furthermore, some studies automate the quantification of snow in PhenoCam images (Caparó Bellido & Rundquist, 2021; Julitta et al., 2014), or the classification of frost (Noh et al., 2021). Many computer vision studies have trained models to classify weather phenomena in domains outside of wildlife cameras (Ibrahim et al., 2019; Jacobs et al., 2009; Lu et al., 2014, 2017; Xiao et al., 2021). However, such models have not been tested in ecological contexts, and the use of a single, efficient classifier to simultaneously detect sunshine and frozen precipitation in wildlife images has not been explored.

Working with wildlife imagery from matching experimental sites in mountains in the northern (Switzerland; CH) and southern (South Africa; ZA) hemispheres, we train ensemble deep learning models to detect micrometeorological conditions of sunshine, hail and snow. Our objectives are as follows: (1) Build a dataset and train deep learning classifiers to derive micrometeorological conditions in images; (2) evaluate different models, data-splitting and ensemble approaches to maximize performance with out-of-sample (same sites, different cameras) and out-of-distribution (different sites, different cameras) test datasets; and (3) demonstrate the application of image-derived micrometeorological variables for ecological research. For this last objective, we classify conditions in almost 2 million unlabelled images in CH and ZA. Then we (i) use snow in ZA images to determine the effects of experimental warming on snow melt, and (ii) use sunshine in CH images to explore the relative importance of sunshine and ambient temperature for bumblebees foraging at high elevations. Our approach efficiently attaches micrometeorological data to remote biodiversity observations. This is particularly useful for biodiversity monitoring in mountains, which are characterized by high levels of endemism, complex topography and microclimatic heterogeneity (Spehn & Körner, 2005).

2 | METHODS

2.1 | Study area

Imaging was carried out over 49 1 × 1 m montane grassland plots across four replicated experimental field sites. In the Calanda massif in the Alps in Switzerland (CH), 24 plots were imaged from June 2021 to October 2021, of which eight were located at a low elevation site (46.869266° N 9.490098° E; 1440 m elevation) and 12 were located at a high-elevation site (46.887824° N 9.489510° E; 2000 m). In the Sentinel region of the Maloti-Drakensberg in South Africa (ZA), 25 subplots were imaged from November 2021 to April 2022, of which five were located at a low elevation site (28.679532° S 28.894816° E; 2200 m) and 20 were located at a high-elevation site (28.754951° S 28.866981° E; 3060 m). The grassland plots we imaged comprised native vegetation, but half of the plots additionally had small plant specimens, of species typical of lower elevations, introduced within them. Half of the high site plots in ZA were also exposed to open-top chamber (OTC) warming of approximately 2°C.

2.2 | Sensor deployment

A Wingscapes TimelapseCam Pro camera (with LED flash) was mounted on a steel frame over each plot, ca. 62 cm from the ground, pointing towards the ground. Each camera captured an area of ca. 30 × 17 cm. All cameras were 'continuous', recording images day and night at 5-min intervals, except for 16 'focused' cameras in CH which recorded at 1-min intervals between 12.00–15.00 and 01.00–03.00 (Alison et al., 2022). Each camera required eight AA lithium batteries and a 128 GB SD card, replaced approximately every 2 months.

All cameras were equipped with on-board temperature sensors, recording temperature at ca. 62 cm above ground with every photograph (either at 5- or 1-min intervals depending on the camera). At the high-elevation sites, we also deployed TMS4 microclimate loggers to record temperature every 15 min at −8, 0 and 15 cm above ground. We deployed loggers in blocks of six, with three blocks at the CH high site and one block at the ZA high site. Each block included two loggers in vegetated plots with OTC warming, two in vegetated plots without warming and one each in bare soil plots with and without OTC warming. Loggers were not targeted to the same plots as cameras, though some of the same plots were sampled by coincidence.

2.3 | Image labelling

We sorted a total of 8953 images into four classes based on micrometeorological conditions: overcast, sunshine, hail or snow (Figure 1; further details in Appendix S1). First, to generate training data representing the entire recording period, we labelled a systematic sample of 6205 images. We sampled one image per hour in both ZA and CH, cycling through the continuous cameras. In CH, we included an additional one image per hour cycling through all focused cameras (5 h per day). The systematic sample yielded 1320 sunshine, 110 snow, 39 hail and 4736 overcast images. Second, to generate adequate training data and improve detection of snow and hail, we took a strategic sample of 2748 images that was informed by the systematic sample. The strategic sampling protocol had three tiers, such that the rarest meteorological events were sampled more intensively (i.e. oversampled; Table S1). The strategic sample yielded an additional set of 266 sunshine, 923 snow, 803 hail and 756 overcast images. CH images were labelled by JA, and ZA images by SP, using VGG Image Annotator (VIA v2.0.11; https://www.robots.ox.ac.uk/~vgg/software/via/).

2.4 | Model training

We trained convolutional neural networks (CNNs) to classify conditions in images as overcast, sunshine, hail or snow using the *Keras* python library (Chollet, 2015). Specifically, we fine-tuned the MobileNet network (Howard et al., 2017) pretrained on ImageNet (Russakovsky et al., 2015), representing a lightweight and efficient family of CNNs that has been shown to perform well for image classification in ecology (Besson et al., 2022; Schneider et al., 2022). To adapt the model to predict just four classes, we removed the top layer of the network and added a custom softmax activation layer with a flattened input. Training images were rescaled to 224 × 224 px and put through an augmentation pipeline to reduce overfitting. Augmentation involved random vertical or horizontal flipping and up to 45° random rotation in any direction. Following preliminary tests, we trained the entire network in two stages using the Adam optimizer and a batch size of 128. First, we trained for five epochs specifying a learning rate of 0.001, to bring models rapidly towards a solution. Second, we trained the entire network for up to 200 epochs, specifying a learning rate of 0.0001. The change in learning rate allowed models to reach an optimal solution while minimizing spurious fluctuations in validation loss. Appendix S2 gives a primer on CNN parameters and concepts.

2.5 | Model validation

We used model validation with early stopping to minimize overfitting to the training data. We stopped training if validation performance did not improve for 30 epochs and saved the model from the epoch with the best validation performance (concepts explained in Appendix S2). To account for variance related to data splitting for validation, we used cross-validation. Specifically, we carried out a fivefold cross-validation in which each of five mutually exclusive data folds is iteratively treated as the validation dataset (e.g. Figure S1, inner validation loop). Additionally, we compared two data-splitting methods: 'Cis' and 'Trans' (Beery et al., 2018, 2020). Cis validation
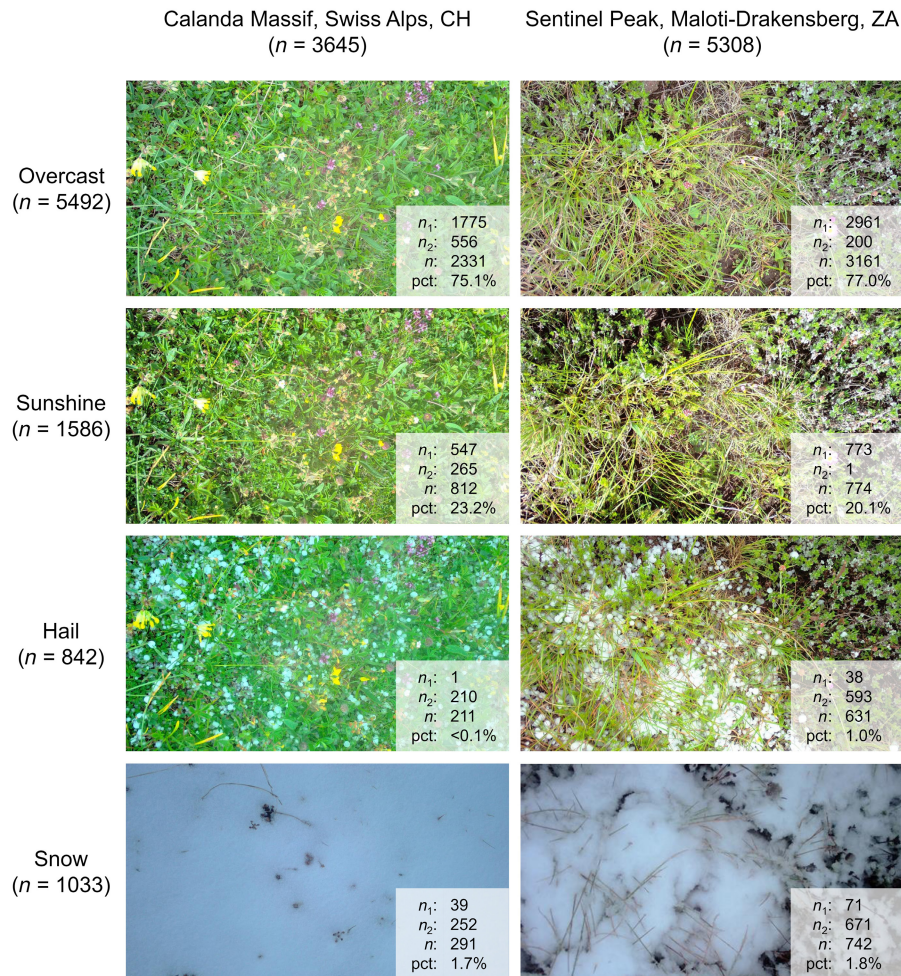
FIGURE 1 Examples of the four classes of micrometeorological conditions in two representative high-elevation plots in Switzerland (CH) and South Africa (ZA). Total numbers of labelled images (*n*) are shown across classes and regions (including high and low elevation sites). The breakdown of labels across the systematic sample (n_1) and the strategic sample (n_2) is also shown, as is the representation of each condition within the systematic sample for a given region (pct).

involves random splitting of images from all cameras. Trans validation splits cameras rather than images, such that images from one camera are always constrained to a single fold (Figure S1). With the Cis validation method, the effective size of the training set is larger, because more camera positions are seen during training. However, the Trans validation method ensures that images from the same camera are not represented in both training and validation data. For both Cis and Trans validation, folds were stratified with respect to the four study sites (Wieczorek et al., 2022).

2.6 | Model aggregation

We produced ensembles of sets of five 'member models', representing the five iterations of each fivefold validation loop, in a procedure called cross-validation aggregation (crogging; Barrow & Crone, 2013; see Appendix S3 for further details). The crogging procedure produces ensemble models in which each observation contributes to both model training (in all but one member model) and model validation

by early stopping (in one member model). Averaging across models which use distinct data folds for validation can improve generalization performance and model stability (Barrow & Crone, 2016; Krogh & Vedelsby, 1994). Ensemble models were produced under both Cis and Trans validation methods. For each fivefold validation loop, five Cis member models and five Trans member models were aggregated into ensembles by unweighted averaging of output softmax probabilities.

2.7 | Model testing and deployment

We aimed for models that would transfer to (1) novel camera positions within our sites and (2) novel sites with a similar recording protocol. To test transferability to novel positions within our sites, each fivefold validation loop was nested within an outer sixfold test loop (e.g. Figure S1). In other words, we used a nested cross-validation or 'double-cross' to obtain a robust and unbiased measure of model generalization (Cawley & Talbot, 2010). We randomly split 49 cameras into six folds that were stratified across the four sites (Wieczorek

et al., 2022). During each test loop iteration, one of sixfold was withheld as a test dataset. We compared model accuracy and macro-F1 (the mean of class F1 scores) following Equations 1–4 where: TP=true positives; TN=true negatives; FP=false positives; FN=false negatives; Pr=class precision; and Re=class recall. Class F1 scores represent class-level performance, and macro-F1 represents overall model performance while accounting for class imbalance.

$$Accuracy = \frac{TP + TN}{TP + FP + TN + FN}. \tag{1}$$

$$Pr = \frac{TP}{TP + FP}. \tag{2}$$

$$Re = \frac{TP}{TP + FN}. \tag{3}$$

$$Class\,F1 = 2\frac{Pr \times Re}{Pr + Re}. \tag{4}$$

To test model transferability to novel sites, we trained two production models by incorporating the test data for training and validation. Specifically, we trained a sixfold Trans ensemble and a sixfold Cis ensemble. Novel site performance was then tested using images from Svalbard, Norway. In a separate study of pollination of *Silene acaulis*, six plots in Bjørndalen (78.21660° N 15.33280° E; 40 m elevation) were imaged at 1-min intervals in June and July 2020 using the same imaging methods. However, some images were cropped slightly to zoom in on *S. acaulis* during annotation. The first 11 images of every hour of every day were labelled for sunshine ($n=957$) and overcast ($n=6222$) conditions by MH. To compare model performance with an existing benchmark, we also classified the Svalbard images using a two-class weather classification model published by Lu et al. (2014, 2017, https://jiaya.me/projects/weatherclassify/index.htm) and deployed in MatLab (The MathWorks Inc., 2023). Data, models and code to train and deploy deep learning models are openly available on Zenodo at https://doi.org/10.5281/zenodo.10137731.

Finally, we deployed our production Trans ensemble model to predict micrometeorological conditions across the full set of 1,934,044 images taken across all four sites in CH and ZA. We validated our time series of micrometeorological conditions against temperature data from TMS4 loggers (Wild et al., 2019). We then analysed micrometeorological conditions to explore (1) effects of OTC warmed and unwarmed treatments on snow cover in ZA, and (2) effects of sensor-derived temperature and image-derived sunshine on *Bombus* visitation to *Trifolium pratense* in CH (using data previously published by Alison et al., 2022). For (2), we calculated the daytime degree days recorded by on-board temperature sensors (sum of mean daily temperatures above 0°C) and sunshine days (sum of mean daily proportional sunshine) during flowering of each inflorescence. We compared AIC of linear models predicting ln(number of visits) of each inflorescence. Furthermore, to investigate mismatch in the microclimatic niches of *T. pratense* and its primary pollinators, we calculated mean temperature and proportional sunshine within an hour either side of each *Bombus* flower visit. This was overlaid on the distribution of temperature and sunshine during daytime hours in which 32 *T. pratense* inflorescences were flowering. Statistical analyses were carried out using *R* (R Core Team, 2023).

3 | RESULTS AND DISCUSSION

Wildlife cameras capture details about species' abiotic environments, and not just their behaviours, life cycles and interactions (Hofmeester et al., 2020). We find that conditions such as sunshine, snow and hail can be readily and automatically extracted from wildlife imagery. Furthermore, we show how such micrometeorological data are complementary to sensor-derived temperature data.

3.1 | Model performance

Ensemble models were highly transferable to novel camera positions, consistently achieving higher accuracy and macro-F1 than member models (Table 1). Ensemble models also outperformed full models, which used all data for training and none for validation, by around 1%. Beyond performance benefits, member models within a given ensemble disagree on 13%–14% of predictions (Table 1) and

TABLE 1 Mean (±SD) performance of full models ($n=6$), ensemble models ($n=6$) and member models ($n=5\times6=30$) in classification of micrometeorological conditions in out-of-sample test images (same sites, different cameras).

Validation split method	Model type	Macro-F1 (%)		Accuracy (%)		Consensus accuracy (%)		Rate of consensus (%)	
Cis	Ensemble	**89.25**	(2.02)	91.63	(1.96)	95.89	(1.69)	87.13	(1.92)
	Member	88.02	(1.59)	90.72	(1.67)				
Trans	Ensemble	88.82	(3.33)	**91.70**	(2.02)	**96.00**	(1.55)	85.90	(3.33)
	Member	87.22	(3.02)	90.41	(2.13)				
None	Full	88.00	(2.61)	90.94	(2.21)				

Note: Performance metrics include macro-F1, accuracy and consensus accuracy for ensemble models. Ensemble models are compared to member models under two validation data split methods: 'Cis' and 'Trans' (see Figure S1). The consensus accuracy of ensemble models is the accuracy of predictions on which all five member models agree. Rate of consensus is the percentage of test images for which all five member models agree. Maxima for macro-F1, accuracy and concensus accuracy are displayed in bold.

this disagreement forms a useful measure of uncertainty; by omitting non-consensus predictions as uncertain, we raised the effective accuracy of our most accurate ensemble to 96%. Differences between models trained using the Cis and Trans validation methods were negligible, while cross-validation revealed considerable variation when models of the same type were trained and tested on different folds of the data (Table 1, see Appendix S3 for further discussion on validation approaches and ensembling). Our models classified overcast and sunshine conditions more successfully than snow or hail (Figure 2; Figure S2), perhaps reflecting the oversampling of snow and hail events. Our ensemble model based on a Trans validation method misclassified 29% of hail images as overcast, 12% of sunshine as overcast and 3% of overcast as sunshine (Figure 2). The apparent bias of the model towards overcast conditions could relate not only to the high variability of that class, but also the over-representation of overcast images in the training data.

The real-world utility of deep learning models hinges on generalization performance, including transferability to novel sites and conditions. When classifying images of *S. acaulis* across six cameras from a totally independent site in Svalbard, Norway, ensemble models using Cis and Trans validation methods distinguished sunshine from overcast conditions with 79.3% and 72.8% accuracy respectively (model F1: 70.9% and 65.0%). Our best model thus outperformed a benchmark model for two-class weather classification, trained on 10,000 images from a variety of outdoor contexts (Lu et al., 2014, 2017), which achieved 75.5% accuracy on Svalbard images. Furthermore, omitting non-consensus predictions as uncertain, we raised the effective accuracy to 94% and 88.4% respectively. Contrary to expectations, when classifying images from Svalbard, ensemble models based on the Cis validation method outperformed those based on the Trans method. This suggests that the reduced overfitting of the Trans ensemble was offset by the reduction in trainin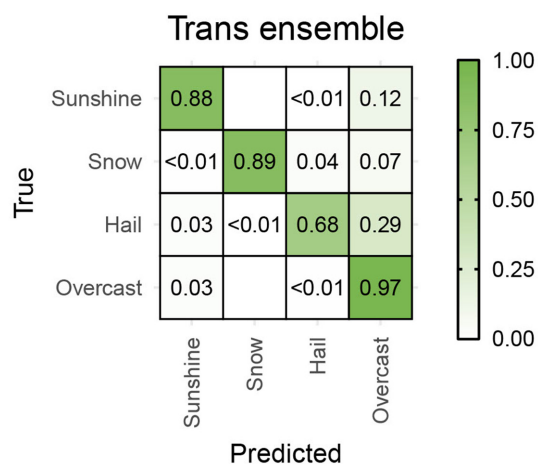g data seen by each member model. Still, the reported generalization performance is impressive given that the out-of-distribution images came from a site >1000 km away, at >1000 m lower elevation, with different height and width compared to training images. For detection of sunshine in images, our models show clear potential to generalize to novel sites with a similar recording protocol.

3.2 | Extensive prediction of micrometeorological data

We predicted micrometeorological conditions in almost 2 million images across CH and ZA sites. Those images were classified by a member model in around 20h on an Intel Xeon E5-2697A v4 processor with 8 CPUs @ ~2.6 GHz. Much faster times would be expected if using a GPU. A consensus prediction emerged for 87.7% of images, and these predictions were averaged across cameras over time to generate seasonal (Figure 3) and diel (Figure 4) micrometeorological profiles. Seasonal profiles revealed a common seasonal pattern of summer hailstorms and autumn snow across mountains in the northern and southern hemispheres (Figure 3). As expected, during the day there was a striking match between image-derived sunshine and sensor-derived temperatures (Figure 3). However, nighttime temperatures also appeared warmer following periods of high daytime cloud cover (i.e. low sunshine before nightfall; Figure 3), as expected under longwave cloud forcing (Ramanathan et al., 1989). Furthermore, diel sunshine profiles revealed that the ZA high-elevation site was characterized by morning sunshine and afternoon shade, with subtle impacts on the diel temperature profile (Figure 4). Such insights would be difficult to obtain without using the meteorological by-catch of wildlife cameras.

3.3 | Effects of experimental warming on snow melt

We found clear impacts of OTCs on the prevalence and duration of snow cover (Figure 5). During the first (and longest) recorded snowfall, the snow melted completely after around 2.5 days in warmed plots. This contrasted with unwarmed plots, where snow persisted for up to 4 days (Figure 5). Beyond temporal variation, we also captured fine-scale spatial variation in retention of snow cover—especially among warmed plots (Figure 5a). Sensor-derived temperatures showed evidence of warming within OTCs, especially during prolonged sunshine, which probably contributed to advanced snow melt. However, snow was often less prevalent across warmed plots even immediately after snowfall (Figure 5). This suggests that OTCs also intercept a fraction of falling snow, which could delay snowpack formation.

Few studies have reported effects of OTCs on snow cover in autumn. Several studies have reported effects on snow depth in winter and snow melt in spring, although observations are often infrequent or anecdotal (Bokhorst et al., 2013; Wipf & Rixen, 2010). Heavy snows are known to accumulate in OTCs over winter, increasing snow depth and insulating plants and soil (Hollister et al., 2023;
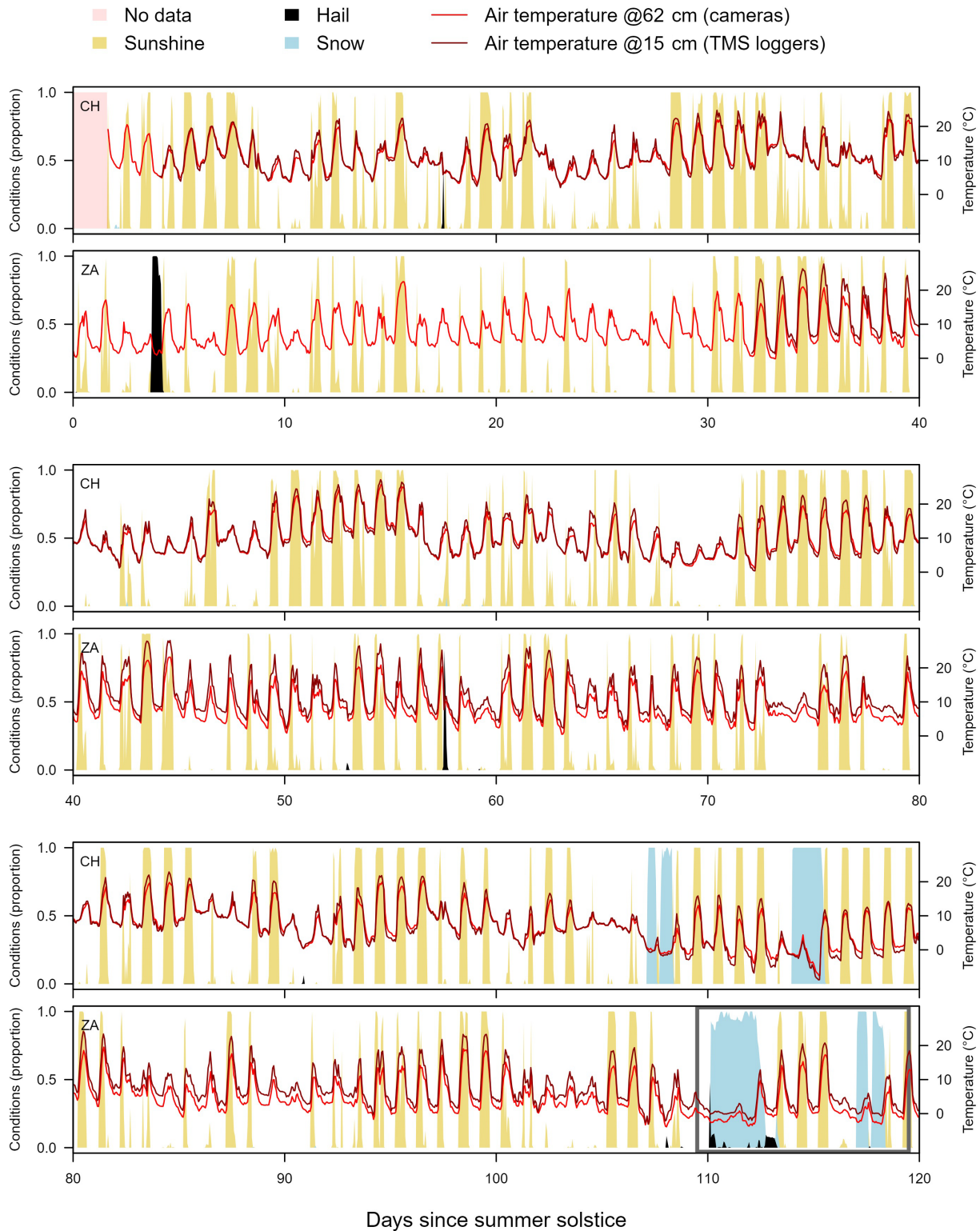

FIGURE 2 Confusion matrix of predicted micrometeorological conditions across 8953 images. Six ensemble deep learning models were used to classify images in six distinct folds of hold-out test cameras in a cross-validation process. Data splitting for validation of these models was done using the Trans validation method (see text and Figure S1 for explanation).

FIGURE 3 Sunshine (yellow), hail (black) and snow (blue) detected in images throughout summer solstice (top pair), early autumn (middle pair) and late autumn (bottom pair) across two mountain sites. Distinct time series from the northern hemisphere (top of each pair) and the southern hemisphere (bottom of each pair) are aligned based on summer solstice dates of 21 June 2021 in Switzerland (CH) and 21 December in South Africa (ZA). Conditions were classified in all images from continuous cameras at the two high-elevation sites, using a deep learning ensemble trained using the full set of 8953 labelled images. Data are displayed with a resolution of 1.2 h (20 time slices per day). We also present mean air temperatures from on-board sensors on cameras, measuring air temperature every 5 min at 62 cm above ground (red lines), and TMS4 loggers, measuring air temperature every 15 min at 15 cm above ground (dark red lines). Data in the grey box (bottom-right) are more closely explored in Figure 5.

Rixen et al., 2022); the resulting winter warming of OTCs often exceeds their spring and summer warming effects (Aerts et al., 2004; Bjorkman et al., 2015). Such snow accumulation leads to unpredictable effects of OTCs on snow melt; it may remain unchanged,
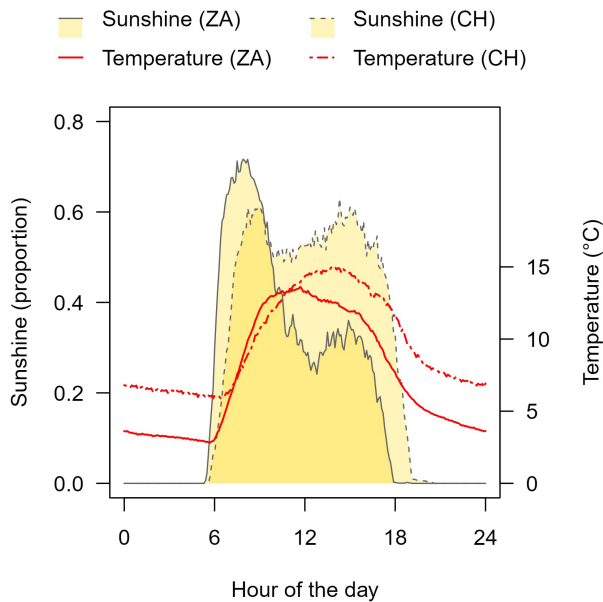
be delayed by a week or be advanced by several weeks (Aerts et al., 2004; Marion et al., 1997; Wipf & Rixen, 2010). Here we show that in early autumn, experimental warming can reduce the duration of snow cover—although this may partly result from interception of snowfall by OTCs. Furthermore, we demonstrate how to efficiently quantify persistence of snow at high spatiotemporal resolutions. This is a vital contribution given the impacts of snow cover on plant and soil ecosystem processes (Möhl et al., 2022), and the prevalence of OTCs in climate change research (Bjorkman et al., 2015; Hollister et al., 2023; Rixen et al., 2022).

3.4 | Effects of sunshine on bumblebee foraging

Sunshine is a vital factor affecting the activity of flower visiting insects, especially in alpine environments (Bergman et al., 1996). Our data demonstrate not only how sunshine drives fluctuations in ambient temperature at our site (Figure 3), but also the cumulative daytime temperatures experienced by individual *T. pratense* inflorescences (Figure 6a). We also observe a strong effect of sunshine exposure on the number of *Bombus* foraging visits to each inflorescence (Figure 6b), probably partly mediated by ambient temperatures. However, we found that sunshine days marginally outperformed degree days when predicting the number of *Bombus* visits to an inflorescence ($\Delta AIC = -0.98$). As such, we suggest that sunshine also has direct effects on *Bombus* foraging activity. For example, solar radiation can directly raise thoracic temperatures of bees, relieving a major constraint on flight behaviour (Corbet et al., 1993).

We overlaid the density of *Bombus* foraging events with the density of flowering *T. pratense* on a two-dimensional surface of sunshine and temperature. Even though *Bombus* visits are contingent on the presence of flowering *T. pratense*, we found evidence of microclimatic and micrometeorological mismatch. *Trifolium pratense* inflorescences were
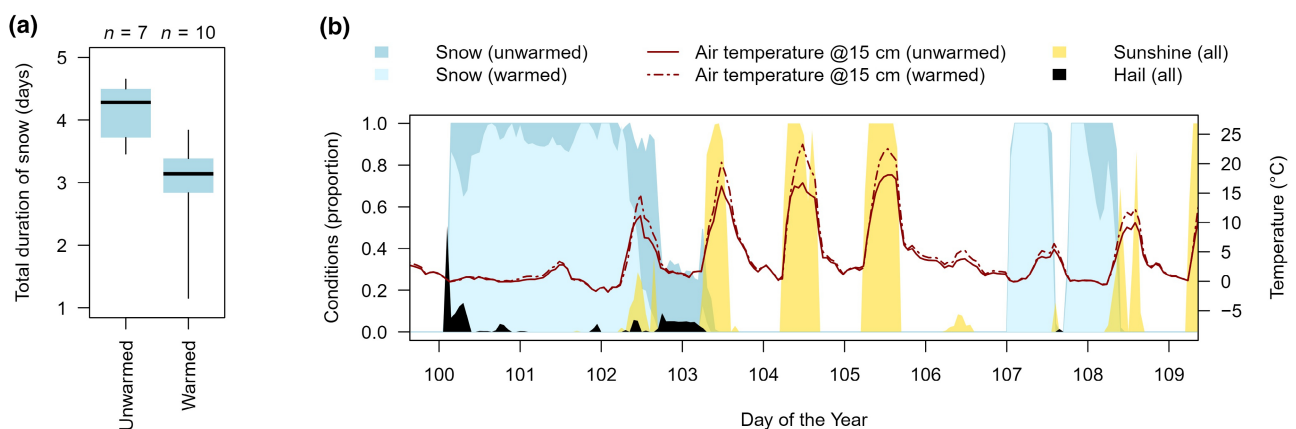

FIGURE 4 Average diel profiles of image-derived sunshine (yellow shading and grey lines) across high-elevation sites in Switzerland (CH, dashed lines) and South Africa (ZA, solid lines) for 120 days following summer solstice. We also present mean air temperatures from on-board sensors on cameras, measuring air temperature every 5 min at 62 cm above ground (red lines). Data are displayed with a resolution of 0.1 h (240 time slices per day). The ZA site is characterized by early morning sunshine and afternoon shade. Sunshine was classified using a deep learning ensemble trained using the full set of 8953 labelled images.

FIGURE 5 (a) Duration of snow, derived from images, across unwarmed plots and open-top chamber (OTC) warmed plots at the high-elevation site in South Africa. Boxes capture the median and interquartile range, while whiskers capture the range of the data. Three cameras failed before the snows and are excluded here. (b) Proportion of snow over time across unwarmed (dark blue) and warmed (light blue) plots. Snow events were often shortened or dampened within OTCs. Furthermore, during periods of sunshine (yellow), temperature spikes recorded by TMS4 loggers were more intense in warmed plots (dashed red line) than unwarmed plots (solid red line). Small proportions of snow images were misclassified as hail (black), and this was often due to fog. Weather conditions were classified using a deep learning ensemble trained using the full set of 8953 labelled images.
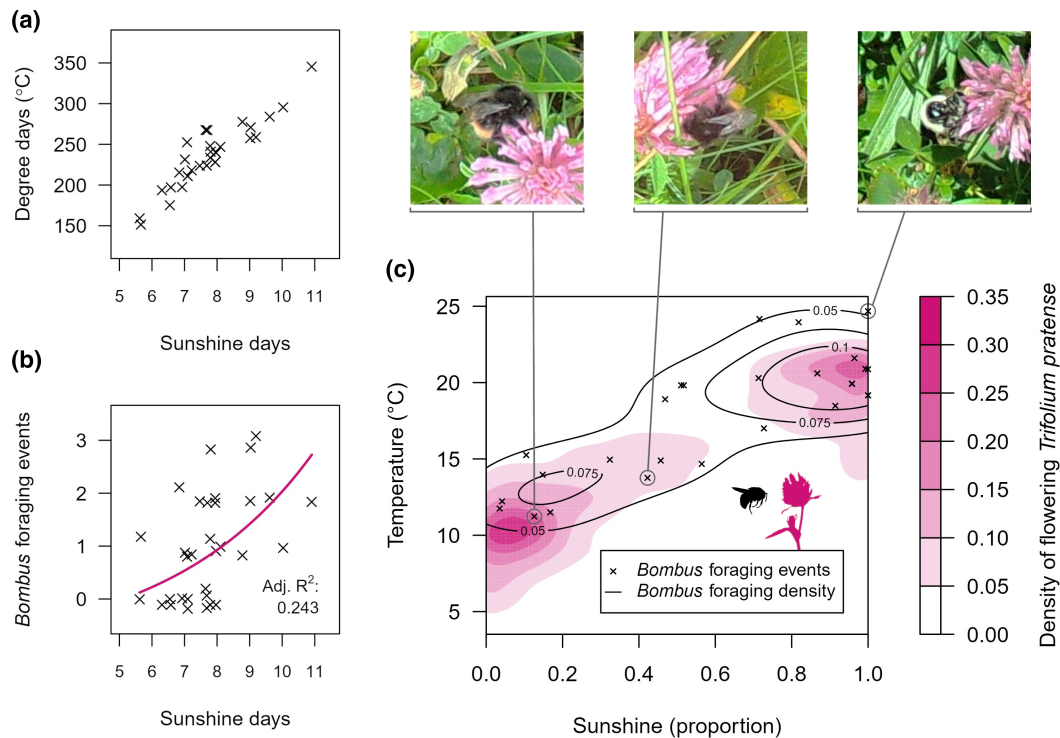
FIGURE 6 (a) The cumulative daytime temperatures experienced by *Trifolium pratense* inflorescences, derived from temperature sensors, are highly positively correlated with sunshine exposure, derived from images. (b) Sunshine exposure of an inflorescence increases the number of recorded *Bombus* foraging events. The pink line represents a linear model that effectively predicts the natural log of the number of *Bombus* foraging events based on the number of days of sunshine received by an inflorescence. (c) Microclimatic and micrometeorological niche overlap between flowering *Trifolium pratense* (pink) and *Bombus* bee pollinators (black contour lines derived from black crosses). The density of flowering *T. pratense* is representative of the underlying distributions of image-derived sunshine and sensor-derived temperature, which are strongly bimodal. In contrast, *Bombus* visits are more concentrated during intermediate sunshine or extremely warm temperatures. Image crops corresponding to three *Bombus* foraging events are shown above the plot.

most available at ~10°C with little or no sunshine, with a secondary peak at ~21°C during constant sunshine (Figure 6c). However, *Bombus* foraging events were completely absent below 10°C, and disproportionately prevalent during intermittent sunshine or extremely warm temperatures. Camera-based monitoring, with automated extraction of meteorological by-catch, allows us to quantify the constraints and preferences of species at unprecedented spatial and temporal resolutions.

3.5 | Applications and future development

Micrometeorological variables extracted from images are highly complementary to those recorded by affordable microclimatic sensors. Unlike temperature and moisture, solar radiation is expensive and difficult to measure at high temporal resolution (Roales et al., 2013). Furthermore, cameras are perhaps the only in-field sensors that can record the prevalence of snow (Caparó Bellido & Rundquist, 2021) and hail at fine spatiotemporal resolutions. Crucially, the impacts of sunshine, snow and hail on the abundance and phenology of wild species are significant, but rarely explored and poorly understood (Fernandes et al., 2011; Möhl et al., 2020, 2022; Valladares et al., 2016). Furthermore, cameras can capture variation in micrometeorology

and organismal activity at very small spatial scales. This creates opportunities to study fine-scale microclimatic refugia, such as areas protected from sunshine or snow, which may be vital for species persistence in extreme environments (von Oppen et al., 2022). Cameras also record continuously at high temporal resolution, allowing the analysis of phenological mismatches not only across days of the year, but also hours of the day (Alison et al., 2022). Finally, cameras generate biological and meteorological data that are tethered in both space and time. This is a particularly useful property to explore behavioural adaptations to micrometeorological conditions.

Previous studies have automated the extraction of snow-covered regions of phenocam images (Caparó Bellido & Rundquist, 2021; Julitta et al., 2014). Our approach of classifying entire images is simpler, and thus broader in application. Our model rapidly identifies not only images with snow, but also those with sunshine or hail. Unlike previous models, ours is shown to perform well on images from novel camera placements and even a distant site in Svalbard. Above all, we present a dataset and methods to train future models that will be even more transferable. Future work should focus on the assembly of larger training datasets, representing a greater diversity of backgrounds, conditions and wildlife camera domains. There is potential for deep learning models to extract hydrological

information from images, for example rainfall or even rare cryogenic processes (Grab et al., 2021). Presenting future models with contextual information, for example the location, time or temperature during image capture, could improve accuracy across a wide range of meteorological conditions (Terry et al., 2020). Still, we show that an existing model, trained on diverse and independent outdoor images, distinguished sunny and overcast images from wildlife cameras with surprising accuracy (Lu et al., 2014, 2017). As such, the roll-out of new and existing weather classification models to extract meteorological by-catch from phenocams for vegetation (Brown et al., 2016) or camera traps for large animals (Hofmeester et al., 2020) is a very exciting prospect. The extraction of latent meteorological information from existing wildlife camera network datasets, containing millions of labelled organisms (Norouzzadeh et al., 2018), could generate new insights into the ecology of a huge variety of animal and plant species worldwide.

AUTHOR CONTRIBUTIONS

ACKNOWLEDGEMENTS

CONFLICT OF INTEREST STATEMENT

The authors have no conflict of interest to declare.

DATA AVAILABILITY STATEMENT

Data, models, and code to train and deploy deep learning models are openly available on Zenodo at https://doi.org/10.5281/zenodo.10137731. Pollinator data is available from Figshare at https://doi.org/10.6084/m9.figshare.20129951.v1.

ORCID

Jamie Alison https://orcid.org/0000-0002-6787-6192
Stephanie Payne https://orcid.org/0000-0002-1493-1506
Jake M. Alexander https://orcid.org/0000-0003-2226-7913
Anne D. Bjorkman https://orcid.org/0000-0003-2174-7800
Vincent Ralph Clark https://orcid.org/0000-0001-5058-0742
Onalenna Gwate https://orcid.org/0000-0003-0237-4316
Evelin Iseli https://orcid.org/0000-0002-1586-8203
Jonathan Lenoir https://orcid.org/0000-0003-0638-9582
Hjalte Mads Rosenstand Mann https://orcid.org/0000-0002-4768-4767
Sandy-Lynn Steenhuisen https://orcid.org/0000-0002-6128-0654
Toke Thomas Høye https://orcid.org/0000-0001-5387-3284

REFERENCES

Aerts, R., Cornelissen, J. H. C., Dorrepaal, E., Van Logtestijn, R. S. P., & Callaghan, T. V. (2004). Effects of experimentally imposed climate scenarios on flowering phenology and flower production of subarctic bog species. *Global Change Biology*, 10(9), 1599–1609. https://doi.org/10.1111/j.1365-2486.2004.00815.x

Alison, J., Alexander, J. M., Zeugin, N. D., Dupont, Y. L., Iseli, E., Mann, H. M. R., & Høye, T. T. (2022). Moths complement bumblebee pollination of red clover: A case for day-and-night insect surveillance. *Biology Letters*, 18, 20220187. https://doi.org/10.1098/rsbl.2022.0187

Antão, L. H., Bates, A. E., Blowes, S. A., Waldock, C., Supp, S. R., Magurran, A. E., Dornelas, M., & Schipper, A. M. (2020). Temperature-related biodiversity change across temperate marine and terrestrial systems. *Nature Ecology & Evolution*, 4(7), 927–933. https://doi.org/10.1038/s41559-020-1185-7

August, T., Harvey, M., Lightfoot, P., Kilbey, D., Papadopoulos, T., & Jepson, P. (2015). Emerging technologies for biological recording. *Biological Journal of the Linnean Society*, 115(3), 731–749. https://doi.org/10.1111/bij.12534

Barrow, D. K., & Crone, S. F. (2013). Crogging (cross-validation aggregation) for forecasting—A novel algorithm of neural network ensembles on time series subsamples. *Proceedings of the International Joint Conference on Neural Networks*. https://doi.org/10.1109/IJCNN.2013.6706740

Barrow, D. K., & Crone, S. F. (2016). Cross-validation aggregation for combining autoregressive neural network forecasts. *International Journal of Forecasting*, 32(4), 1120–1137. https://doi.org/10.1016/j.ijforecast.2015.12.011

Beery, S., Liu, Y., Morris, D., Piavis, J., Kapoor, A., Meister, M., Joshi, N., & Perona, P. (2020). Synthetic examples improve generalization for rare classes. *Proceedings—2020 IEEE Winter Conference on Applications of Computer Vision*, WACV 2020, pp. 852–862. https://doi.org/10.1109/WACV45572.2020.9093570

Beery, S., Van Horn, G., & Perona, P. (2018). Recognition in Terra Incognita. *Lecture Notes in Computer Science (Including Subseries Lecture Notes in*

Artificial Intelligence and Lecture Notes in Bioinformatics), 11220 LNCS, pp. 472–489. https://doi.org/10.1007/978-3-030-01270-0_28

Bergman, P., Molau, U., & Holmgren, B. (1996). Micrometeorological impacts on insect activity and plant reproductive success in an alpine environment, Swedish Lapland. *Arctic and Alpine Research*, 28(2), 196–202. https://doi.org/10.2307/1551760

Besson, M., Alison, J., Bjerge, K., Gorochowski, T. E., Høye, T. T., Jucker, T., Mann, H. M. R., & Clements, C. F. (2022). Towards the fully automated monitoring of ecological communities. *Ecology Letters*, 25(12), 2753–2775. https://doi.org/10.1111/ele.14123

Bjorkman, A. D., Elmendorf, S. C., Beamish, A. L., Vellend, M., & Henry, G. H. R. (2015). Contrasting effects of warming and increased snowfall on Arctic tundra plant phenology over the past two decades. *Global Change Biology*, 21(12), 4651–4661. https://doi.org/10.1111/gcb.13051

Bokhorst, S., Huiskes, A., Aerts, R., Convey, P., Cooper, E. J., Dalen, L., Erschbamer, B., Gudmundsson, J., Hofgaard, A., Hollister, R. D., Johnstone, J., Jónsdóttir, I. S., Lebouvier, M., Van de Vijver, B., Wahren, C. H., & Dorrepaal, E. (2013). Variable temperature effects of open top chambers at polar and alpine sites explained by irradiance and snow depth. *Global Change Biology*, 19(1), 64–74. https://doi.org/10.1111/gcb.12028

Brown, T. B., Hultine, K. R., Steltzer, H., Denny, E. G., Denslow, M. W., Granados, J., Henderson, S., Moore, D., Nagai, S., SanClements, M., Sánchez-Azofeifa, A., Sonnentag, O., Tazik, D., & Richardson, A. D. (2016). Using phenocams to monitor our changing earth: Toward a global phenocam network. *Frontiers in Ecology and the Environment*, 14(2), 84–93. https://doi.org/10.1002/fee.1222

Burton, A. C., Neilson, E., Moreira, D., Ladle, A., Steenweg, R., Fisher, J. T., Bayne, E., & Boutin, S. (2015). Wildlife camera trapping: A review and recommendations for linking surveys to ecological processes. *Journal of Applied Ecology*, 52(3), 675–685. https://doi.org/10.1111/1365-2664.12432

Caparó Bellido, A., & Rundquist, B. C. (2021). Semi-automatic fractional snow cover monitoring from near-surface remote sensing in grassland. *Remote Sensing*, 13(11), Article 11. https://doi.org/10.3390/rs13112045

Cawley, G. C., & Talbot, N. L. C. (2010). On over-fitting in model selection and subsequent selection bias in performance evaluation. *Journal of Machine Learning Research*, 11, 2079–2107.

Chollet, F. (2015). *Keras* [computer software]. https://keras.io

Corbet, S. A., Fussell, M., Ake, R., Fraser, A., Gunson, C., Savage, A., & Smith, K. (1993). Temperature and the pollinating activity of social bees. *Ecological Entomology*, 18(1), 17–30. https://doi.org/10.1111/j.1365-2311.1993.tb01075.x

Fernandes, G. W., Oki, Y., Sanchez-Azofeifa, A., Faccion, G., & Amaro-Arruda, H. C. (2011). Hail impact on leaves and endophytes of the endemic threatened *Coccoloba cereifera* (Polygonaceae). *Plant Ecology*, 212(10), 1687–1697. https://doi.org/10.1007/s11258-011-9941-z

Gillespie, M. A. K., Baggesen, N., & Cooper, E. J. (2016). High Arctic flowering phenology and plant–pollinator interactions in response to delayed snow melt and simulated warming. *Environmental Research Letters*, 11(11), 115006. https://doi.org/10.1088/1748-9326/11/11/115006

Gillespie, M. A. K., & Cooper, E. J. (2022). The seasonal dynamics of a high Arctic plant–visitor network: Temporal observations and responses to delayed snow melt. *Arctic Science*, 8(3), 786–803. https://doi.org/10.1139/as-2020-0056

Grab, S., Knight, J., Mol, L., Botha, T., Carbutt, C., & Woodborne, S. (2021). Periglacial landforms in the high Drakensberg, southern Africa: Morphogenetic associations with rock weathering rinds and shrub growth patterns. *Geografiska Annaler: Series A, Physical Geography*, 103(3), 199–222. https://doi.org/10.1080/04353676.2020.1856625

Hofmeester, T. R., Young, S., Juthberg, S., Singh, N. J., Widemo, F., Andrén, H., Linnell, J. D. C., & Cromsigt, J. P. G. M. (2020). Using by-catch data from wildlife surveys to quantify climatic parameters and timing of phenology for plants and animals using camera traps. *Remote Sensing in Ecology and Conservation*, 6(2), 129–140. https://doi.org/10.1002/rse2.136

Hollister, R. D., Elphinstone, C., Henry, G. H. R., Bjorkman, A. D., & Klanderud, K. (2023). A review of open top chamber (OTC) performance across the ITEX network. *Arctic Science*, 9(2), 1–14.

Howard, A. G., Zhu, M., Chen, B., Kalenichenko, D., Wang, W., Weyand, T., Andreetto, M., & Adam, H. (2017). MobileNets: Efficient convolutional neural networks for Mobile vision applications. *arXiv*, http://arxiv.org/abs/1704.04861

Høye, T. T., Ärje, J., Bjerge, K., Hansen, O. L. P., Iosifidis, A., Leese, F., Mann, H. M. R., Meissner, K., Melvad, C., & Raitoharju, J. (2021). Deep learning and computer vision will transform entomology. *Proceedings of the National Academy of Sciences of the United States of America*, 118(2), 1–10. https://doi.org/10.1073/PNAS.2002545117

Ibrahim, M. R., Haworth, J., & Cheng, T. (2019). WeatherNet: Recognising weather and visual conditions from street-level images using deep residual learning. *ISPRS International Journal of Geo-Information*, 8(12), Article 12. https://doi.org/10.3390/ijgi8120549

Intergovernmental Panel on Climate Change (Ed.). (2023). Weather and climate extreme events in a changing climate. In *Climate change 2021—The physical science basis: Working Group I Contribution to the Sixth Assessment Report of the Intergovernmental Panel on Climate Change* (pp. 1513–1766). Cambridge University Press. https://doi.org/10.1017/9781009157896.013

Jacobs, N., Burgin, W., Fridrich, N., Abrams, A., Miskell, K., Braswell, B. H., Richardson, A. D., & Pless, R. (2009). The global network of outdoor webcams: Properties and applications. *Proceedings of the 17th ACM SIGSPATIAL International Conference on Advances in Geographic Information Systems*, pp. 111–120. https://doi.org/10.1145/1653771.1653789

Julitta, T., Cremonese, E., Migliavacca, M., Colombo, R., Galvagno, M., Siniscalco, C., Rossini, M., Fava, F., Cogliati, S., Morra di Cella, U., & Menzel, A. (2014). Using digital camera images to analyse snowmelt and phenology of a subalpine grassland. *Agricultural and Forest Meteorology*, 198–199, 116–125. https://doi.org/10.1016/j.agrformet.2014.08.007

Katal, N., Rzanny, M., Mäder, P., & Wäldchen, J. (2022). Deep learning in plant phenological research: A systematic literature review. *Frontiers in Plant Science*, 13, 805738. https://doi.org/10.3389/fpls.2022.805738

Krogh, A., & Vedelsby, J. (1994). Neural network ensembles, cross validation, and active learning. *Advances in Neural Information Processing Systems*, 7, 231–238.

Lembrechts, J. J., Aalto, J., Ashcroft, M. B., De Frenne, P., Kopecký, M., Lenoir, J., Luoto, M., Maclean, I. M. D., Roupsard, O., Fuentes-Lillo, E., García, R. A., Pellissier, L., Pitteloud, C., Alatalo, J. M., Smith, S. W., Björk, R. G., Muffler, L., Ratier Backes, A., Cesarz, S., … Nijs, I. (2020). SoilTemp: A global database of near-surface temperature. *Global Change Biology*, 26(11), 6616–6629. https://doi.org/10.1111/gcb.15123

Lembrechts, J. J., Lenoir, J., Roth, N., Hattab, T., Milbau, A., Haider, S., Pellissier, L., Pauchard, A., Ratier Backes, A., Dimarco, R. D., Nuñez, M. A., Aalto, J., & Nijs, I. (2019). Comparing temperature data sources for use in species distribution models: From in-situ logging to remote sensing. *Global Ecology and Biogeography*, 28(11), 1578–1596. https://doi.org/10.1111/geb.12974

Lenoir, J., Bertrand, R., Comte, L., Bourgeaud, L., Hattab, T., Murienne, J., & Grenouillet, G. (2020). Species better track climate warming in the oceans than on land. *Nature Ecology & Evolution*, 4(8), 1044–1059. https://doi.org/10.1038/s41559-020-1198-2

Lu, C., Lin, D., Jia, J., & Tang, C.-K. (2014). Two-class weather classification. *2014 IEEE Conference on Computer Vision and Pattern Recognition*, pp. 3718–3725. https://doi.org/10.1109/CVPR.2014.475

Lu, C., Lin, D., Jia, J., & Tang, C.-K. (2017). Two-class weather classification. *IEEE Transactions on Pattern Analysis and Machine Intelligence*, *39*(12), 2510–2524. https://doi.org/10.1109/TPAMI.2016.2640295

Lumbrazo, C., Bennett, A., Currier, W. R., Nijssen, B., & Lundquist, J. (2022). Evaluating multiple canopy-snow unloading parameterizations in SUMMA with time-lapse photography characterized by citizen scientists. *Water Resources Research*, *58*(6), e2021WR030852. https://doi.org/10.1029/2021WR030852

Maclean, I. M. D., Duffy, J. P., Haesen, S., Govaert, S., De Frenne, P., Vanneste, T., Lenoir, J., Lembrechts, J. J., Rhodes, M. W., & Van Meerbeek, K. (2021). On the measurement of microclimate. *Methods in Ecology and Evolution*, *12*(8), 1397–1410. https://doi.org/10.1111/2041-210X.13627

Maclean, I. M. D., & Early, R. (2023). Macroclimate data overestimate range shifts of plants in response to climate change. *Nature Climate Change*, *13*(5), 484–490. https://doi.org/10.1038/s41558-023-01650-3

Mann, H. M. R., Iosifidis, A., Jepsen, J. U., Welker, J. M., Loonen, M. J. J. E., & Høye, T. T. (2022). Automatic flower detection and phenology monitoring using time-lapse cameras and deep learning. *Remote Sensing in Ecology and Conservation*, *1–13*, 765–777. https://doi.org/10.1002/rse2.275

Marion, G. M., Henry, G. H. R., Freckman, D. W., Johnstone, J., Jones, G., Jones, M. H., Lévesque, E., Molau, U., Mølgaard, P., Parsons, A. N., Svoboda, J., & Virginia, R. A. (1997). Open-top designs for manipulating field temperature in high-latitude ecosystems. *Global Change Biology*, *3*(Suppl. 1), 20–32. https://doi.org/10.1111/j.1365-2486.1997.gcb136.x

Möhl, P., Hiltbrunner, E., & Körner, C. (2020). Halving sunlight reveals no carbon limitation of aboveground biomass production in alpine grassland. *Global Change Biology*, *26*(3), 1857–1872. https://doi.org/10.1111/gcb.14949

Möhl, P., von Büren, R. S., & Hiltbrunner, E. (2022). Growth of alpine grassland will start and stop earlier under climate warming. *Nature Communications*, *13*(1), Article 1. https://doi.org/10.1038/s41467-022-35194-5

Noh, I., Doh, H.-W., Kim, S.-O., Kim, S.-H., Shin, S., & Lee, S.-J. (2021). Machine learning-based hourly frost-prediction system optimized for orchards using automatic weather station and digital camera image data. *Atmosphere*, *12*(7), Article 7. https://doi.org/10.3390/atmos12070846

Norouzzadeh, M. S., Nguyen, A., Kosmala, M., Swanson, A., Palmer, M. S., Packer, C., & Clune, J. (2018). Automatically identifying, counting, and describing wild animals in camera-trap images with deep learning. *Proceedings of the National Academy of Sciences of the United States of America*, *115*(25), E5716–E5725. https://doi.org/10.1073/pnas.1719367115

Ortmann, C. R., & Johnson, S. D. (2021). How reliable are motion-triggered camera traps for detecting small mammals and birds in ecological studies? *Journal of Zoology*, *313*(3), 202–207. https://doi.org/10.1111/jzo.12849

Pecl, G. T., Araújo, M. B., Bell, J. D., Blanchard, J., Bonebrake, T. C., Chen, I.-C., Clark, T. D., Colwell, R. K., Danielsen, F., Evengård, B., Falconi, L., Ferrier, S., Frusher, S., Garcia, R. A., Griffis, R. B., Hobday, A. J., Janion-Scheepers, C., Jarzyna, M. A., Jennings, S., … Williams, S. E. (2017). Biodiversity redistribution under climate change: Impacts on ecosystems and human well-being. *Science*, *355*(6332), eaai9214. https://doi.org/10.1126/science.aai9214

Potter, K. A., Arthur Woods, H., & Pincebourde, S. (2013). Microclimatic challenges in global change biology. *Global Change Biology*, *19*(10), 2932–2939. https://doi.org/10.1111/gcb.12257

R Core Team. (2023). *R: A language and environment for statistical computing* [computer software]. R Foundation for Statistical Computing.

Ramanathan, A. V., Cess, R. D., Harrison, E. F., Minnis, P., Barkstrom, B. R., Ahmad, E., Hartmann, D., Science, S., Series, N., Jan, N., Ramanathan, V., Cess, R. D., Harrison, E. F., Minnis, P., Barikstrom, B. R., Ahmad, E., & Hartmann, D. (1989). Cloud-radiative forcing and climate: Results from the earth radiation budget experiment. *Science*, *243*(4887), 57–63.

Rixen, C., Høye, T. T., Macek, P., Aerts, R., Alatalo, J. M., Jill, T., Arnold, P. A., Barrio, I. C., Bjerke, J. W., Björkman, M. P., Blok, D., Blumewerry, G., Boike, J., Bokhorst, S., Carbognani, M., Christiansen, C. T., Convey, P., Cooper, E. J., Cornelissen, J. H. C., … Zong, S. (2022). Winters are changing: Snow effects on Arctic and alpine tundra ecosystems. *Arctic Science*, *8*(February), 572–608.

Roales, J., Durán, J., Bechtold, H. A., Groffman, P. M., & Rosi-Marshall, E. J. (2013). High resolution measurement of light in terrestrial ecosystems using photodegrading dyes. *PLoS ONE*, *8*(9), e75715. https://doi.org/10.1371/journal.pone.0075715

Russakovsky, O., Deng, J., Su, H., Krause, J., Satheesh, S., Ma, S., Huang, Z., Karpathy, A., Khosla, A., Bernstein, M., Berg, A. C., & Fei-Fei, L. (2015). ImageNet large scale visual recognition challenge. *International Journal of Computer Vision*, *115*(3), 211–252. https://doi.org/10.1007/s11263-015-0816-y

Schneider, S., Taylor, G. W., Kremer, S. C., Burgess, P., McGroarty, J., Mitsui, K., Zhuang, A., deWaard, J. R., & Fryxell, J. M. (2022). Bulk arthropod abundance, biomass and diversity estimation using deep learning for computer vision. *Methods in Ecology and Evolution*, *13*(2), 346–357. https://doi.org/10.1111/2041-210X.13769

Spehn, E. M., & Körner, C. (2005). A global assessment of mountain biodiversity and its function. In U. M. Huber, H. K. M. Bugmann, & M. A. Reasoner (Eds.), *Global change and mountain regions: An overview of current knowledge* (pp. 393–400). Springer Netherlands. https://doi.org/10.1007/1-4020-3508-X_39

Terry, J. C. D., Roy, H. E., & August, T. A. (2020). Thinking like a naturalist: Enhancing computer vision of citizen science images by harnessing contextual data. *Methods in Ecology and Evolution*, *11*(2), 303–315. https://doi.org/10.1111/2041-210X.13335

The MathWorks Inc. (2023). *MATLAB Version: 23.2.0.2409890 (R2023b) Update 3* [computer software].

Tuia, D., Kellenberger, B., Beery, S., Costelloe, B. R., Zuffi, S., Risse, B., Mathis, A., Mathis, M. W., van Langevelde, F., Burghardt, T., Kays, R., Klinck, H., Wikelski, M., Couzin, I. D., van Horn, G., Crofoot, M. C., Stewart, C. V., & Berger-Wolf, T. (2022). Perspectives in machine learning for wildlife conservation. *Nature Communications*, *13*(1), 1–15. https://doi.org/10.1038/s41467-022-27980-y

Valladares, F., Laanisto, L., Niinemets, Ü., & Zavala, M. A. (2016). Shedding light on shade: Ecological perspectives of understorey plant life. *Plant Ecology and Diversity*, *9*(3), 237–251. https://doi.org/10.1080/17550874.2016.1210262

von Oppen, J., Assmann, J. J., Bjorkman, A. D., Treier, U. A., Elberling, B., Nabe-Nielsen, J., & Normand, S. (2022). Cross-scale regulation of seasonal microclimate by vegetation and snow in the Arctic tundra. *Global Change Biology*, *28*(24), 7296–7312. https://doi.org/10.1111/gcb.16426

Wevers, J., Beenaerts, N., Casaer, J., Zimmermann, F., Artois, T., & Fattebert, J. (2021). Modelling species distribution from camera trap by-catch using a scale-optimized occupancy approach. *Remote Sensing in Ecology and Conservation*, *7*(3), 534–549. https://doi.org/10.1002/rse2.207

Wieczorek, J., Guerin, C., & McMahon, T. (2022). K-fold cross-validation for complex sample surveys. *Stat*, *11*(1), e454. https://doi.org/10.1002/sta4.454

Wild, J., Kopecký, M., Macek, M., Šanda, M., Jankovec, J., & Haase, T. (2019). Climate at ecologically relevant scales: A new temperature and soil moisture logger for long-term microclimate measurement. *Agricultural and Forest Meteorology*, *268*, 40–47. https://doi.org/10.1016/j.agrformet.2018.12.018

Wipf, S., & Rixen, C. (2010). A review of snow manipulation experiments in Arctic and alpine tundra ecosystems. *Polar Research*, *29*(1), 95–109. https://doi.org/10.1111/j.1751-8369.2010.00153.x

Xiao, H., Zhang, F., Shen, Z., Wu, K., & Zhang, J. (2021). Classification of weather phenomenon from images by using deep convolutional neural network. *Earth and Space Science*, *8*(5), e2020EA001604. https://doi.org/10.1029/2020EA001604

SUPPORTING INFORMATION

Additional supporting information can be found online in the Supporting Information section at the end of this article.